Environmental Science & Technology

pubs.acs.org/est

Article

Phenotypic and Transcriptional Responses of *Pseudomonas aeruginosa* Biofilms to UV-C Irradiation via Side-Emitting Optical Fibers: Implications for Biofouling Control

Zhe Zhao, Yi-Hao Luo,* Tzu-Heng Wang, Shahnawaz Sinha, Li Ling, Bruce Rittmann, Pedro Alvarez, François Perreault, and Paul Westerhoff*

Cite This: *Environ. Sci. Technol.* 2023, 57, 15736−15746

Read Online

ACCESS | Metrics & More | Article Recommendations | Supporting Information

ABSTRACT: Biofilms give rise to a range of issues, spanning from harboring pathogens to accelerating microbial-induced corrosion in pressurized water systems. Introducing germicidal UV-C (200−280 nm) irradiation from light-emitting diodes (LEDs) into flexible side-emitting optical fibers (SEOFs) presents a novel light delivery method to inhibit the accumulation of biofilms on surfaces found in small-diameter tubing or other intricate geometries. This work used surfaces fully submerged in flowing water that contained *Pseudomonas aeruginosa*, an opportunistic pathogen commonly found in water system biofilms. A SEOF delivered a UV-C gradient to the surface for biofilm inhibition. Biofilm growth over time was monitored *in situ* using optical conference tomography. Biofilm formation was effectively inhibited when the 275 nm UV-C irradiance was ≥8 μW/cm^2. Biofilm samples were collected from several regions on the surface, representing low and high UV-C irradiance. RNA sequencing of these samples revealed that high UV-C irradiance inhibited the expression of functional genes related to energy metabolism, DNA repair, quorum sensing, polysaccharide production, and mobility. However, insufficient sublethal UV-C exposure led to upregulation genes for SOS response and quorum sensing as survival strategies against the UV-C stress. These results underscore the need to maintain minimum UV-C exposure on surfaces to effectively inhibit biofilm formation in water systems.

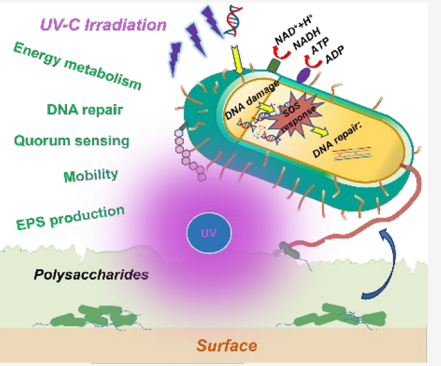

KEYWORDS: *side-emitting optical fiber, UV-C, biofilm inhibition, transcriptional response*

1. INTRODUCTION

Biofilms in water systems can cause fouling and microbially induced corrosion (MIC), and pathogenic microorganisms harbored within biofilms (e.g., *Legionella pneumophila*) pose human health risks;[1] these impacts sum to $3 trillion per year in costs worldwide.[2] Ultraviolet-C (UV-C) irradiation from light-emitting diodes (LEDs) is a chemical-free process that is highly biocidal to planktonic pathogens and has been proven to minimize biofilm formation on surfaces.[3−5] However, delivering UV-C light to complex surfaces (e.g., drinking water pipes, cooling tower basins, point-of-use devices, biomedical devices) is difficult because optical obstructions lower the UV-C light irradiance from the design value, making the actual UV-C irradiation insufficient to minimize biofilm formation on surfaces.[6]

Previous research has shown that UV-C irradiation can reduce the level of biofilm formation. Torkzadeh et al. concluded that UV-C at 254 nm and 50 μW/cm^2 reduces biofilm formation at 20 °C by 95% over 48 h; an even lower UV-C irradiance is required to achieve the same reduction at low temperature (<10 °C) due to the lower bacterial growth rate.[7,8] Cells collected from established biofilms were inactivated by UV-C with wavelengths from 220 to 285 nm at a total dose of ∼40 mJ/cm^2.[4,9,10] Inactivation was attributed to nucleic-acid damage by UV-C direct exposure.[5] Despite the positive results in those studies, generalizable findings are absent due to (1) UV-C light irradiance not being experimentally constant across different reactor configurations and (2) lack of information on gene expression in biofilms responding to UV-C light. Providing data to address these gaps can be a first step in comparing UV-C irradiation to chemical-based (i.e., silver, chlorine) biofilm control.[11,12]

We overcame both experimental limitations by connecting the UV-C light source to side-emitting optical fibers (SEOFs) to create continuous and controllable UV-C irradiance from 0 to ∼250 μW/cm^2.[13] SEOFs are thin (<500 μm) and flexible optical fibers designed to transmit and side-emit germicidal

Received: June 16, 2023
Revised: September 13, 2023
Accepted: September 14, 2023
Published: October 6, 2023

https://doi.org/10.1021/acs.est.3c04658
Environ. Sci. Technol. 2023, 57, 15736−15746

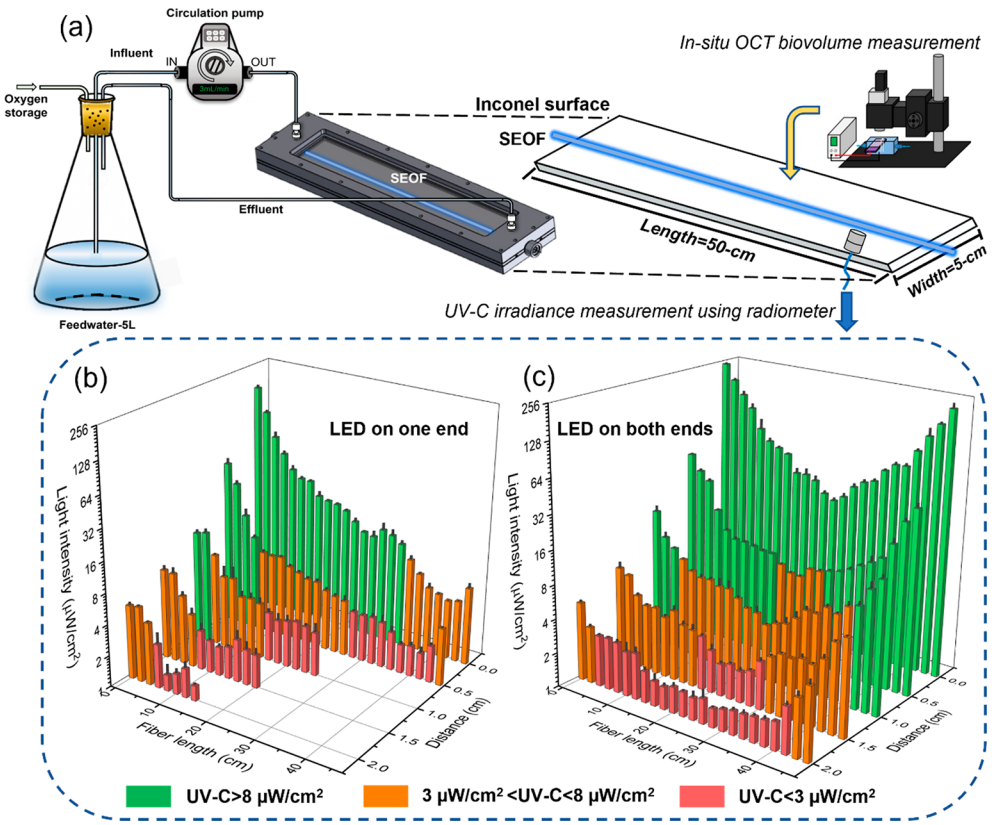

Figure 1. (a) Experimental setup for growing biofilm in a 50 cm-long reactor with irradiation from a single SEOF delivering UV-C light from one end or both ends. UV-C irradiance from (b) the LED on one end or (c) the LEDs on both ends measured at different distances from and along the length of the single SEOF.

light, like *glowsticks*, when attached to a light emitting diode (LED) light source, and have lifespans expected to be longer than 10 years based upon their composition and stability in different environments.[14] Germicidal SEOFs have been shown to inhibit biofilm formation on surfaces and to inactivate planktonic bacteria in water.[14−16] Furthermore, the level of UV-C irradiance transmitted through the SEOFs can be adjusted by modifying the SEOFs' surface, either by coating nanoparticles as light scattering centers or by modulating UV-C transparent polymers to create more or less side emission.[17,18] Here, we applied SEOFs in fully submerged, flow-through, stainless steel reactors with a nutrient rich water spiked with *Pseudomonas aeruginosa*, an opportunistic pathogen commonly found in water systems,[19] to evaluate biofilm accumulation and transcriptional response under varying UV-C irradiance.

Using continuous-flow biofilm reactors, we answered two research questions: (1) What is the minimum UV-C irradiance to inhibit biofilm accumulation and (2) How do *P. aeruginosa* biofilms respond to varying UV-C irradiance compared to a control without light? A 50 cm long biofilm reactor was fabricated with an SEOF that could deliver UV-C irradiance ranging from 0 to ∼250 μW/cm^2 to a stainless-steel surface along the reactor length. Biofilm inhibition kinetics under UV-C light were monitored over time using optical coherence tomography (OCT) to calculate average biofilm thickness (mm) on surfaces. RNA from biofilm samples collected from three surface regions of variable UV-C irradiance (<5 μW/cm^2, >8 μW/cm^2, and >250 μW/cm^2 for 30 min irradiation) were reverse transcribed to DNA, which was sequenced to indicate which genes were differentially expressed in response to UV-C exposure. The selected genes were related to DNA repair, quorum sensing, mobility, and biofilm formation, which would inspire future studies of targeting the biofilm inhibition strategy.

2. MATERIALS AND METHODS

2.1. Microbial Culture Preparation. *Pseudomonas aeruginosa* (ATCC 15692, Manassas, Virginia) was used as model biofilm-forming bacteria for its ability to rapidly grow biofilms on surfaces and its pathogenic nature.[20] An overnight culture was diluted 1:25 in LB broth and incubated at 37 °C until the optical density at 600 nm reached 1 cm^{-1}; this gave a bacterial suspension with a concentration of approximately 10^9 CFU/mL. The suspension was diluted 1:1000 into M9 medium as feedwater for biofilm forming experiments. Details about the M9 medium are shown in Table SI.1. The M9 medium enables interference-free microscope imaging, which was suitable for OCT analysis in this work. At the beginning of each experiment, the feedwater was placed in a 5-L volumetric flask with an initial *P. aeruginosa* concentration of $10^{5.7\pm0.1}$ CFU/mL.

2.2. Biofilm Reactor Design and UV-C Exposures from SEOFs. Figure 1a shows a schematic of the reactor used to form a biofilm and deliver UV-C via SEOFs. A photograph of the experimental device is shown in Figure SI.1. The 55 cm long biofilm reactor was watertight and had a light-transparent quartz window for *in situ* imaging via OCT microscopy. A 50 cm × 5 cm stainless steel (Inconel 625, HPALLOY, IN) metal plate was placed inside the reactor as the surface for biofilm

https://doi.org/10.1021/acs.est.3c04658
Environ. Sci. Technol. 2023, 57, 15736−15746

formation. Inconel stainless steel is widely used in water systems (i.e., tanks, piping, cooling towers) and has been previously proven to accumulate biofilm rapidly.[21,22]

A single 50 cm custom-made quartz SEOF was inserted on the top of the Inconel surface in the same way as the apparatus reported in previous study.[23] A fixed spacing (~0.3 cm) was intentionally maintained between SEOF and the Inconel surface, and therefore any grown biofilms were perpendicular to the UV-C light side emitted from the SEOF (Figure SI.2). Fiber characteristics were 0.39 numerical aperture, 500-μm diameter, and 1.5 core refractive index (Polymicron, Phoenix, AZ). Fiber cut-ends were cleaned by an optical cleaner (Vytran, Thorlabs, NJ) to create a smooth surface for light transmission. SEOFs were connected to UV-C LEDs (80 mW) housed in a custom-designed integrated device (PearlLab FiberBeam, Aquasense Technologies, Kentucky, USA; Figure SI.3c) on both ends to create surface UV-C exposure. Figure SI.3 shows a representative picture of SEOF glowing at one end or both ends inside the reactor. Details of the fiber fabrication and how it was connected to UV-C LEDs are given by Zhao et al.[13] The UV-C emission from SEOFs was measured with a spectrophotoradiometer (AvaSpec461 2048L, Avantes, Louisville, CO). Light irradiance (μW/cm^2) along the 50 cm optical fiber (L, cm) was measured at distances of 0, 0.5, 1.0, 1.5, and 2.0 cm perpendicular to the fiber surface (d, cm) and taken as the UV-C irradiance exposed onto the biofilm formed on the surface. The radiometer's detection limit was 1 μW/cm^2.

The feedwater containing *P. aeruginosa* was recirculated through the 55 cm reactor at 3 mL/min for 72 h. Figure SI.4 shows that the feedwater concentration during the recirculation ranged from $10^{5.7\pm0.1}$ to $10^{7.1\pm0.1}$ CFU/mL. Because the only UV-C irradiation in this experimental setup was from the fiber, planktonic bacteria in feedwater experienced low UV-C irradiation only when they were inside the reactor. Based upon the volumetric flow rate and residence time in the reactor, very low planktonic bacterial inactivation occurred in the flowing water. A dark control experiment was performed by using the same reactor design, including an SEOF, but without UV-C irradiation from LEDs; all other experimental conditions (i.e., surface, flow rate, time, and feedwater) were maintained the same. Experiments with and without UV-C light were performed in triplicate.

2.3. Biofilm Surface Average Thickness Analysis. *In-situ* biofilm formation on the surface during the recirculation period was measured every 24 h using OCT focused through the quartz window following the protocol described in our previous work.[16] OCT images were analyzed using a 3D viewer and Voxel Counter Plugins with ImageJ. Biofilm average thickness (equals volume of biomass (mm^3) per unit surface (mm^2)) at locations near the fiber surface (0 cm away from the SEOF) and 2 cm away from the SEOF was recorded every 4 cm along the 50 cm length.

2.4. Biofilm Collection and Treatment for RNA Extraction and Reverse-Transcriptase Sequencing. A sterile brush was used to collect duplicated biofilm samples from four different zones in the 50 cm reactors, with or without side-emitting light as shown in Figure SI.5. Table SI.2 describes the four samples. Two biofilm samples were collected after recirculating water for 72 h in a reactor without SEOF irradiation. One sample was directly analyzed (i.e., *dark control*), and another sample was first subjected to 30 min UV-C irradiation by a low-pressure UV lamp (ThermoFisher, Model # 51032328, LPUV, 40 V) that delivered 250 μW/cm^2 to the biofilm surface (i.e., *Post UV-C exposed* biofilm) before collection. The other two samples were collected from the reactor exposed to UV-C from the SEOF; the sample location zones were at different distances and corresponded to either 8−80 μW/cm^2 (i.e., *Effectively Inhibited* biofilms) or <3 μW/cm^2 (i.e., *Poorly inhibited* biofilms).

Each sample prepared for RNA extraction was stored in RNAlater (Thermo Fisher Scientific, US) solution at −20 °C. A TRIzol Max Bacterial RNA Isolation Kit (Thermo Fisher Scientific, US) was used to extract the RNA from all biofilm samples. The extracted RNA was purified with a MICROBExpress Kit (Thermo Fisher Scientific, US) to remove ribosome RNA. Then, the mRNA was reverse transcribed to cDNA using a High-Capacity cDNA Reverse Transcription Kit (Applied Biosystems, US). All cDNA samples were shipped overnight in a cooler to CosmosID Inc. (MD, USA) for shallow metagenomic sequencing. Details of the cDNA sample preparation and sequencing are listed in the Text SI.1.

After sequencing, the "Trimmomatic" tool was used to remove low-quality reads (sequence length < 60 bp; quality score < 30) from all cDNA sequencing reads.[24] The detailed quality of the cDNA sequencing reads before and after quality control (QC) for each sample is listed in Table SI.3. To investigate the transcriptional response of biofilms to UV-C exposure, we used the "UProC" toolbox to classify all samples' cDNA sequencing reads based on the KEGG (Kyoto Encyclopedia of Genes and Genomes) database.[25] All cDNA reads were translated into amino acids sequences. Then, the obtained oligopeptide sequences (protein-level) were identified based on the "Mosaic Matching Score" best-matched protein family. The relative abundance of functional categories is presented as transcripts per million (TPM). The calculation method and definition of TPM were reported by Wagner et al. (2012).[26] The $\log_2$fold changes of TPM of different samples represent the response of genes in biofilms irradiated by UV-C light relative to the response for the dark control biofilm sample.

2.5. Statistical Analyses. All of the experiments were performed independently in triplicate using three different SEOFs. For RNA sequencing, duplicate samples were collected separately. Student's t test was used to determine statistical significance. Differences were considered as significant at the 95% confidence level ($p < 0.05$).

3. RESULTS AND DISCUSSION

3.1. SEOFs Irradiated Axial UV-C Gradient onto the Surface Biofilms. UV-C light side-emitted along the length of an SEOF, transmitted into water, and delivered onto the reactor surfaces exponentially attenuates once the light leaves the fiber. Therefore, a UV-C "gradient" is generated axially along the length of the SEOFs and perpendicular to the SEOF. Figure 1b shows the light irradiance along the SEOF connected to the UV-C LED; Figure SI.6 shows irradiance data along and perpendicular to the SEOF. At the fiber surface, the side emission (I_{SEOF}) varied from 156 ± 8 μW/cm^2 at the proximal end (L = 0 cm) to 4 ± 1 μW/cm^2 at the terminal end (L = 48 cm). Light irradiance was lower at distances farther away from the SEOF. For example, at the proximal end, UV-C irradiance decreased from 156 ± 8 μW/cm^2 at d = 0 cm to 5 ± 0.4 μW/cm^2 at d = 2 cm. Overall, UV-C irradiance inside the reactor with only one end of SEOF connected to the LED was

https://doi.org/10.1021/acs.est.3c04658
Environ. Sci. Technol. 2023, 57, 15736−15746

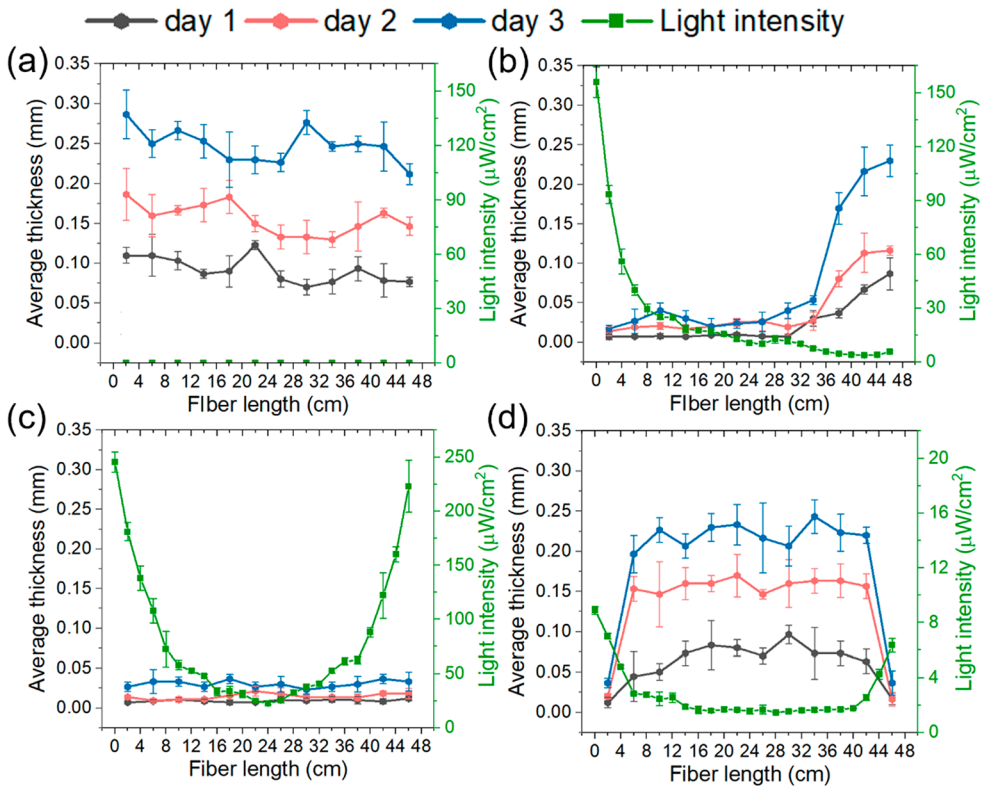

Figure 2. UV-C irradiance (I_{SEOF}) measured at the SEOF surface (green symbols and lines) and biofilm thickness over time (1, 2, and 3 days) along the length of the reactors (L = 0 is the influent proximal end) and adjacent to the SEOF (d = 0 cm) for (a) control reactor in the dark (SEOF without an LED), (b) reactor with SEOF connected to one LED, (c) reactor with SEOF connected to 2 LEDs adjacent to the SEOF (d = 0 cm offset), and (d) reactor with SEOF connected to 2 LEDs at d = 2 cm offset perpendicular from the SEOF. Biofilm average thickness calculated from 3D OCT images shown in Figure SI.7.

highest at L = 0 cm and d = 0 cm and continuously decreased to zero at L = 46 cm and d = 2 cm.

Figures 1c and SI.6 show the light irradiance when LEDs were connected on both ends. A "U-shape" light distribution was created near the fiber surface; I_{SEOF} decreased from 246 ± 9 μW/cm^2 at the proximal end (L = 0 cm) to 24 ± 1 μW/cm^2 in the middle (L = 24 cm) and then continuously increased to 224 ± 20 μW/cm^2 at the terminal end (L = 46 cm). The light irradiances decayed at distances away from fiber surface following the same trend as that at d = 0 cm for one-end illumination. Therefore, UV-C irradiance inside the reactor with LEDs on both ends maximized at L = 0 cm, d = 0 cm and at L = 46 cm, d = 0 cm, and it minimized at L = 24 cm, d = 2 cm.

3.2. Biofilm Formation Was Inhibited on Surfaces by Applying >8 μW/cm^2 UV-C Irradiance. Biofilm formation in reactors exposed to UV-C irradiances was monitored *in situ* through OCT. Nutrient rich media with planktonic bacteria continuously recirculated across the reactor surface. As such, there was a continuous supply of live bacteria available to attach to the surface, as well as continuous shedding of biological material from the surface due to the low shear force of the flowing water. OCT is a technique used to quantify variations in optical density. Previously applied to biofilms on surfaces, OCT effectively distinguishes between water, biofilms, and metal surfaces due to their distinct refractive indices.[16,23,27] Herein the OCT was employed to estimate and monitor the relative disparities in biofilm thickness during in-operando conditions (i.e., without removing biofilms from the reactor), leveraging these refractive index distinction. Figure SI.7a shows the three-dimensional OCT images of biofilm along the surface without UV-C irradiation, and Figure 2a shows the corresponding calculated average biofilm thicknesses. Because the bacterial concentration in the recirculating solution was maintained >10^6 CFU/mL during the experiment (Figure SI.4), any differences in biofilm accumulation on the surface can be attributed to the UV-C light emitted from the SEOF. Biofilms were uniform on the surface from day 1 to day 3, approaching 0.25 ± 0.05 mm on day 3. The obtained average thickness was similar to previous work using a similar biofilm reactor.[16]

Delivering UV-C light to the reactor surface significantly decreased the level of biofilm accumulation. The UV-C irradiance (Figure 1b) and biofilm inhibition zones (Figure 2) were both conical in shape, covering a larger surface area near the proximal end of the reactor and smaller surface area near the terminal end. Figure 2b shows the calculated average thicknesses along the length of the SEOF (biofilm OCT images provided in Figure SI.7b). From L = 0 cm to L = 34 cm, there was a biofilm inhibition zone, where only thin biofilm formed (0.02 ± 0.004 to 0.04 ± 0.01 mm). There was no evidence of biofilm formation on the optical fiber surface, and the side emission from the fiber remained consistent both prior to and subsequent to the recirculation process (Figure SI.8). There was no statistically significant difference in the biofilm thickness within the inhibition zone. Consistent with work using similar flow reactors, sufficient UV-C irradiation inhibited biofilm accumulation (i.e., near-zero thicknesses) but did not sterilize the surface.[16,28]

https://doi.org/10.1021/acs.est.3c04658
Environ. Sci. Technol. 2023, 57, 15736−15746

With LEDs on both ends, I_{SEOF} levels > 20 $\mu W/cm^2$ were achieved along the entire 50 cm length of the SEOF surface (Figure 1c). Consequently, biofilms near the SEOF were inhibited everywhere within the reactor (Figure 2c). To confirm the biofilm response to UV light, the average thickness at 2 cm away from the SEOF was analyzed (Figure 2d), as this location had significantly less UV-C irradiance. The obtained average thickness was consistent with previous results: biofilm was well-controlled at the ends, with irradiance equal to ~8 $\mu W/cm^2$ but accumulated in all other places that had negligible UV-C irradiation (i.e., ~2 $\mu W/cm^2$).

Based on biofilm growth during the experiment, biofilm specific growth rates (μ, day^{-1}) for the different UV-C irradiances were calculated based using eq 1:

$$\frac{dX(t)}{dt} = \mu X(t) \quad (1)$$

where $X(t)$ is biofilm average thickness (mm) at time t (days), μ is the specific biofilm growth rate (day^{-1}), which was influenced by UV light. Figure SI.9 summarizes all measured biofilm thicknesses at different locations in the reactors that had unique UV-C irradiances. Figure 3 shows the calculated

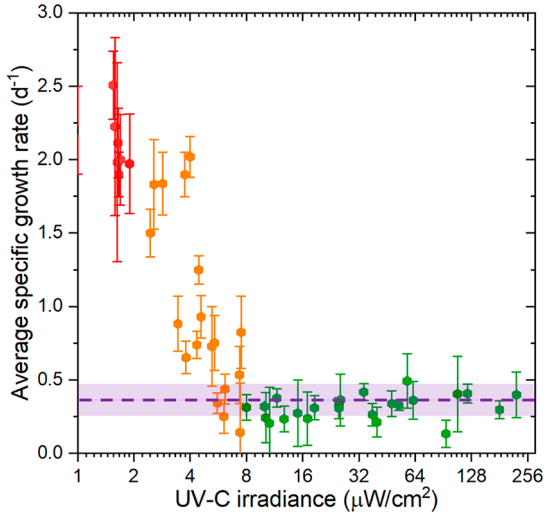

Figure 3. Biofilm specific growth rates in the 50 cm reactor where SEOFs delivered different UV-C irradiance to the reactor surface. The purple shaded region represents the average and 95% confidence interval (μ = 0.34 ± 0.06 day^{-1}) of the specific growth rates when biofilm was *effectively inhibited* (green symbols). Orange symbols represent biofilm specific growth rates in the transitional range (3 < UV-C < 8 $\mu W/cm^2$) when biofilm was *partly inhibited*. Red symbols represent biofilm growth rates when the biofilm was *poorly inhibited*.

biofilm specific growth rates over the 3-day experiments. Without UV-C exposure, the biofilm thickness was 0.25 ± 0.05 mm and had an average specific growth rate of 2.2 ± 0.3 day^{-1} over 72 h. Biofilm growth inhibition began (i.e., lower growth rate and average thickness) in the presence of UV-C. Biofilm growth rates with UV-C fell into three regions: (1) UV-C > 8 $\mu W/cm^2$ where biofilm is *effectively inhibited* and characterized by a low growth rate (average μ value of 0.3 day^{-1}), (2) UV-C < 3 $\mu W/cm^2$ where biofilm is *poorly inhibited* with statistically similar specific growth rates to that in dark control without light, or (3) a transitional UV-C range (3 < UV-C < 8 $\mu W/cm^2$) where biofilm is *partly inhibited*. Figure SI.10 shows the represented live/dead cell ratios for biofilms collected from these areas. The point where UV-C irradiance results in biofilm specific growth rates becoming statistically different (i.e., beyond 95% confidence interval) from 0.3 day^{-1} was considered the UV-C irradiance required to effectively inhibit biofilm, defined as UV_{min}.

Statistically similar and small biofilm thickness (i.e., 0.03 ± 0.02 mm) and specific growth rates (i.e., μ = 0.3 ± 0.1 day^{-1}) occurred at locations within the reactor where irradiance > 8 $\mu W/cm^2$. Further increases in UV-C irradiance did not lead to less biofilm accumulation or a slower specific growth rate, indicating that distributing light energy over a larger area is more practical than focusing high-dose UV-C irradiation in a small area. Overall, surfaces exposed to ≥8 $\mu W/cm^2$ UV-C irradiance had minimal biofilm accumulation, showing OCT-based thickness near detection limits and below 0.02 mm. Values of UV_{min} are likely unique to the organism, nutrient levels, temperature, shear forces, and other conditions; while kept constant in this study, these conditions would likely differ under other scenarios. Because UV_{min} effectively inhibited biofilm formation, surfaces in the reactor exposed to UV-C above 8 $\mu W/cm^2$ provided a marginal or negligible additional benefit.

3.3. Transcriptional Response of *P. aeruginosa* to the UV-C Irradiation. Although UV-C irradiation significantly inhibited biofilm accumulation when the irradiance was >8 $\mu W/cm^2$, some bacteria survived in a thin biofilm layer. Biofilm samples were collected from four locations after 3 days (Table SI.2). At the time of collection, biofilms may have contained previously deposited bacteria that were inactivated or inhibited by UV-C exposure plus bacteria recently deposited to the surface from planktonic organisms in water recirculating through the reactor. Biofilms that had no exposure to UV-C irradiation (see details in Materials and Methods) were compared with two other types of biofilms: (1) samples collected from reactor regions where biofilm was *effectively inhibited* by continuous UV-C intensity (i.e., 8 $\mu W/cm^2$ < UV-C < 80 $\mu W/cm^2$) or *poorly inhibited* (i.e., < 3 $\mu W/cm^2$) and (2) established biofilm collected from the reactor without UV-C exposure (*dark control*) and then postexposed to UV-C light (250 $\mu W/cm^2$ for 30 min). The relative abundance of sequenced mRNA read (transcripts per million (TPM)) represents a snapshot of gene expression information at the time of biofilm sample collection.[29]

3.3.1. Energy Metabolism. Gene expression related to ATP and NADH synthesis is plotted in heatmaps in Table 1. Most genes were downregulated by 3.5- to 0.7-log_2fold for biofilms postexposed to UV-C light. Downregulation of genes responsible for ATP and NADH synthesis demonstrates suppression of basic energy metabolism in the bacteria. Higher UV-C exposure has the potential to hinder the microbial activity of biofilms by impeding their energy metabolism. On the contrary, both inhibited biofilm samples collected from regions in the reactor where biofilms were either *effectively inhibited* or *poorly inhibited* were mostly upregulated, which suggests that surviving bacteria increased energy processing. Compared to the negative control, the divergent transcriptional responses among different UV-C exposed biofilms indicate that high UV-C exposure was required to impede energy metabolism. The elevated energy processing resulting from inadequate UV-C exposure might conceivably play a role in driving other bacterial phenotypic responses to UV-C exposure.

https://doi.org/10.1021/acs.est.3c04658
Environ. Sci. Technol. 2023, 57, 15736−15746

Table 1. Effects of Post-Treatment (UV-C > 250 μW/cm^2), *Effectively Inhibited* (8 μW/cm^2 < UV-C < 80 μW/cm^2), and *Poorly Inhibited* (UV-C < 3 μW/cm^2) UV-C Irradiation on *P. aeruginosa* Biofilm Gene Expression Relative to Dark Control (No UV-C Exposure) for Energy Metabolism (i.e., ATP and NADH synthesis) and DNA Damage and SOS Response[a]

	Gene	KO number	Function	Log$_2$fold change relative to dark control		
				Post-treatment UV-C exposure biofilm	Continuous UV-C irradiance that *effectively inhibited* biofilm growth	Continuous UV-C irradiance that *poorly inhibited* biofilm growth
Energy metabolism	*atpG*	*K02115*	F-type H+-transporting ATPase subunit gamma	-1.3	0.6	0.8
	atpB	*K02108*	F-type H+-transporting ATPase subunit a	-1.7	1.9	1.2
	atpE	*K02110*	F-type H+-transporting ATPase subunit c	-3.1	0.9	1.4
	atpC	*K02114*	F-type H+-transporting ATPase subunit epsilon	-2.2	1.8	0.4
	atpD	*K02112*	F-type H+/Na+-transporting ATPase subunit beta	-1.2	1.3	1.4
	atpF	*K02109*	F-type H+-transporting ATPase subunit b	-1.2	2.1	1.5
	nuoL	*K00341*	NADH-quinone oxidoreductase subunit L	-1.4	0.1	1.0
	nuoJ	*K00339*	NADH-quinone oxidoreductase subunit J	-1.1	1.0	1.1
	nuoG	*K00336*	NADH-quinone oxidoreductase subunit G	-1.8	0.8	0.7
	nuoE	*K00334*	NADH-quinone oxidoreductase subunit E	-0.7	1.6	3.1
	nuoB	*K00331*	NADH-quinone oxidoreductase subunit B	-2.1	1.5	0.8
	nuoM	*K00342*	NADH-quinone oxidoreductase subunit M	-2.1	0.8	-0.3
	nuoF	*K00335*	NADH-quinone oxidoreductase subunit F	-2.0	-0.7	-0.8
	nuoI	*K00338*	NADH-quinone oxidoreductase subunit I	-2.9	0.3	-2.6
DNA damage and SOS response	*herA*	*K06915*	DNA double-strand break repairhelicase related ATPase	-1.9	-2.0	0.4
	mutM	*K10563*	formamidopyrimidine-DNA glycosylase	-1.7	-1.3	-0.2
	recA	*K03553*	recombination protein RecA	-2.4	1.0	-0.4
	recD	*K03581*	exodeoxyribonuclease V alpha subunit	-2.1	0.0	0.6
	recG	*K03655*	ATP-dependent DNA helicase RecG	-1.7	-1.3	0.3
	recJ	*K07462*	single-stranded-DNA-specific exonuclease	-1.5	-0.1	0.9
	recO	*K03584*	DNA repair protein RecO	-0.8	0.8	2.1
	sbcD	*K03547*	DNA repair protein SbcD/Mre11	-1.6	0.3	0.8
	uvrD	*K03657*	DNA helicase II / ATP-dependent DNA helicase	-1.0	0.4	0.2

[a]The color gradient from blue to red indicates the relative expression level log$_2$fold changes of different stages compared to the dark control, with scales ranging from −3.1 to +3.1.

3.3.2. SOS Gene Response and DNA Damage. The SOS gene response is a global regulatory system that responds to DNA damage and repairs the DNA.[30,31] The gene expression levels of SOS-response genes, plotted in Table 1, revealed complete downregulation of DNA-repairing genes in UV-C postexposed biofilms, which means that exposure of a pre-established biofilm to the very high UV-C caused so much DNA damage that it inhibited DNA repair. For biofilm collected from the *effectively inhibited* regions, the gene encoding recombination protein *RecA* was 1-log$_2$fold upregulated, as were DNA-repair genes *recO*, *sbcD*, and *uvrD*. However, SOS-response genes were down-regulated, which suggests that the UV-C irradiation in that area did not allow bacterial repair of DNA damage. For biofilm collected from the *poorly inhibited* regions, most of the DNA-repair genes were upregulated, which may have been important for helping the bacteria survive the DNA damage from moderate UV-C irradiation.

3.3.3. Quorum Sensing, Polysaccharide Biosynthesis, and Mobility. While a SOS gene response triggers DNA repair to overcome DNA damage, quorum sensing is another regulation system that might protect bacteria from UV-C irradiation stress by enhancing adherence, motility, extracellular matrix synthesis, and eventually biofilm formation.[32] In quorum sensing, *P. aeruginosa* bacteria sense and respond to their population density using signal molecules (e.g., N-acylated homoserine lactones (acyl-HSL)).[33,30] The gene expression levels of two acyl-HSL signaling systems (*las* and *rhl*) in three different zones are plotted in Table 2. Both quorum-sensing systems were downregulated for biofilm samples postexposed to UV-C light. For biofilm collected from the *effectively inhibited* regions, *lasR/lasI* and *rhlR/rhlI* were upregulated by 1.9/3.0-log$_2$fold and 2.0/0.6-log$_2$fold, respectively. From the *poorly inhibited* regions, less upregulation of the two systems was observed than that in biofilms collected from *effectively inhibited* regions.

The upregulation of quorum sensing genes should promote biofilm formation by increasing the production of *LecA/LecB* lectins. *LecA* contributes to the *P. aeruginosa* biofilm formation by cross-linking galactosides on the surface of different

https://doi.org/10.1021/acs.est.3c04658
Environ. Sci. Technol. 2023, 57, 15736−15746

Table 2. Effects of Post-Treatment (UV-C > 250 μW/cm^2), *Effectively Inhibited* (8 μW/cm^2< UV-C < 80 μW/cm^2), and *Poorly Inhibited* (UV-C < 3 μW/cm^2) UV-C Irradiance on *P. aeruginosa* Biofilm Gene Expression Relative to Dark Control (No UV-C Exposure) for Quorum Sensing, Polysaccharide and Lipopolysaccharide Synthesis, and Mobility[a]

	Gene	KO number	Function	Log$_2$fold change relative to dark control		
				Post-treatment UV-C exposure biofilm	Continuous UV-C irradiance that *effectively inhibited* biofilm growth	Continuous UV-C irradiance that *poorly inhibited* biofilm growth
Quorum sensing	*lasR*	*K18304*	LuxR family transcriptional regulator, quorum-sensing system regulator LasR	-0.3	1.9	1.2
	lasI	*K13060*	acyl homoserine lactone synthase	0.0	3.0	0.4
	rhlR	*K18099*	LuxR family transcriptional regulator, quorum-sensing system regulator RhlR	-0.2	2.0	0.6
	rhlI	*K13061*	acyl homoserine lactone synthase	-0.4	0.6	-0.1
	lecA	*K20258*	PA-I galactophilic lectin	-2.4	0.2	-1.0
	lecB	*K20277*	mannose-binding lectin	NA	NA	NA
polysaccharide and lipopolysaccharide	*pelC*	*K21008*	polysaccharide biosynthesis protein PelC	-1.2	-0.6	0.5
	pelD	*K21009*	polysaccharide biosynthesis protein PelD	-0.6	0.1	1.4
	pelE	*K21010*	polysaccharide biosynthesis protein PelE	-0.8	-0.3	1.6
	plsC	*K25205*	polysaccharide biosynthesis protein PslC	-0.5	-0.6	2.7
	pslL	*K21005*	polysaccharide biosynthesis protein PslL	-2.1	-1.5	0.7
	wbpA	*K13015*	UDP-N-acetyl-D-glucosamine dehydrogenase	-4.5	1.0	-0.1
	wbpD	*K13018*	UDP-2-acetamido-3-amino-2,3-dideoxy-glucuronate N-acetyltransferase	-3.5	0.8	-0.2
	wbpE	*K13017*	UDP-2-acetamido-2-deoxy-ribo-hexuluronate aminotransferase	-5.4	0.8	-0.8
	wbpG	*K24326*	aminotransferase	-5.6	1.6	-0.9
	wbpI	*K13019*	UDP-GlcNAc3NAcA epimerase	-3.3	2.1	0.6
Mobility	*flgF*	*K02391*	flagellar basal-body rod protein FlgF	-0.6	1.7	-0.4
	flhF	*K02404*	flagellar biosynthesis protein FlhF	-0.4	0.4	1.2
	fliD	*K02407*	flagellar hook-associated protein 2	-0.4	2.4	1.5
	fliM	*K02416*	flagellar motor switch protein FliM	-0.6	1.4	1.2
	fliO	*K02418*	flagellar protein FliO/FliZ	-1.1	0.5	1.3
	fliS	*K02422*	flagellar secretion chaperone FliS	-1.5	0.5	0.9
	chpD	*K06599*	AraC family transcriptional regulator, chemosensory pili system protein ChpD	-1.0	-0.4	1.2
	fimA	*K07345*	major type 1 subunit fimbrin (pilin)	-1.7	-0.6	1.1
	fimT	*K08084*	type IV fimbrial biogenesis protein FimT	-4.5	-0.5	0.5
	fimU	*K08085*	type IV fimbrial biogenesis protein FimU	-2.7	-3.4	0.1

[a]The color gradient from blue to red indicates the relative expression level log$_2$fold changes of different stages compared to the dark control, with scales ranging from −6.8 to +3.1. "NA" stands for "none-appliable" when zero expression was detected for dark control but positive TPM was obtained for other samples.

bacterial cells.[34] *LecB* binds to specific carbohydrate ligands located at the bacterial cell surface, which could enhance the adhesion of *P. aeruginosa* and enable colonization and biofilm formation.[35] The gene *LecA* was downregulated with −2.4-log$_2$fold for the postexposed biofilm and −1.0-log$_2$fold for biofilms collected from the *effectively inhibited* regions. The gene *LecB* was upregulated from 0 to >300 TPM for *effectively inhibited* regions and >100 TPM for *poorly inhibited* regions. *LecB* could be a key factor that enhances *P. aeruginosa* biofilm formation under the stress of UV-C irradiation.

The polysaccharide biosynthesis genes (*pel* and *psl*) were mostly downregulated for biofilm collected from the *effectively inhibited* regions, but they were upregulated in the *poorly inhibited* regions (Table 2). However, the lipopolysaccharide biosynthesis genes (*wbp*) were upregulated for *effectively inhibited* regions, but they were downregulated for *poorly inhibited* regions. Lipopolysaccharides and polysaccharides are protective extracellular exopolysaccharides that can promote biofilm formation.[36,37] The different regulation in response to irradiation suggests that higher UV-C irradiation promoted the biosynthesis of lipopolysaccharide, while lower UV-C irradiation promoted polysaccharide. The results suggest that lipopolysaccharides and polysaccharides may contribute to the bacterial defense in different scenarios.

Table 2 shows the flagellar synthesis genes were upregulated from 0.4 to 2.4-log$_2$fold in samples collected from the *effectively inhibited* regions and upregulated from 0.9 to 1.5-log$_2$fold in *poorly inhibited* regions. Bacterial flagella propel the bacterial cells and can lead to motility for the bacteria cell to escape from the stress of UV-C irradiation.[38,39] UV-C post-treatment of a pre-established biofilm inhibited the expression of flagella-synthesis genes. Biofilm samples from both the *effectively* and *poorly inhibited* regions promoted motility genes in the bacteria.

Different from flagella, pili and fimbriae of bacteria promote surface adhesion.[40,41] The downregulation of pili and fimbriae

https://doi.org/10.1021/acs.est.3c04658
Environ. Sci. Technol. 2023, 57, 15736−15746

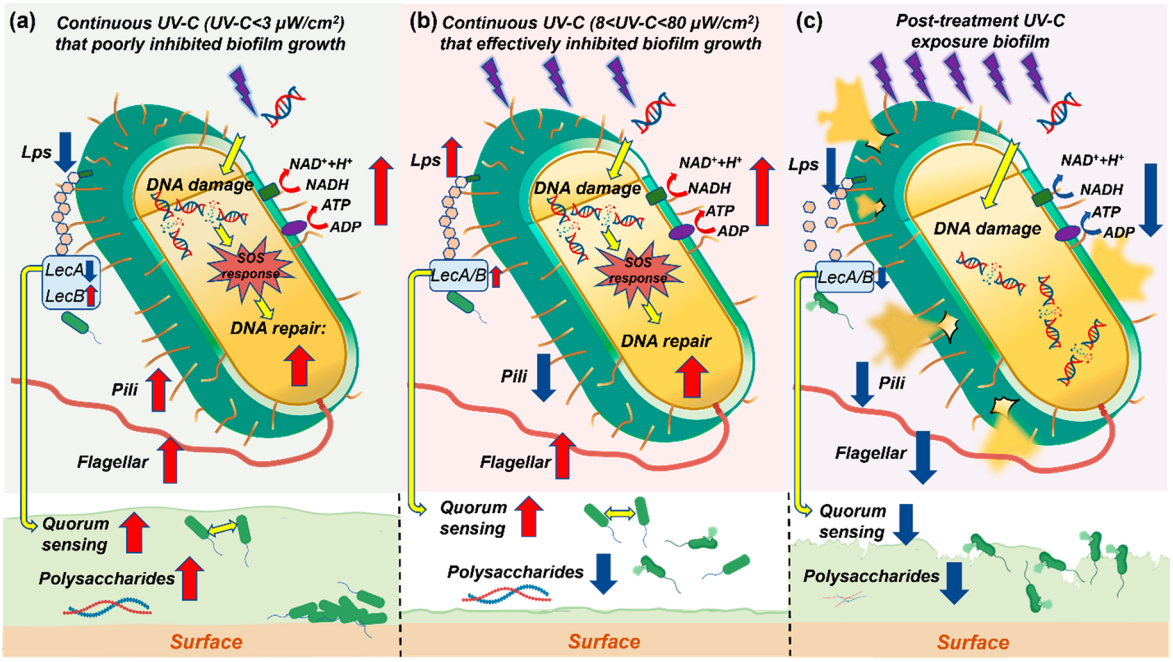

Figure 4. Schematics of *P. aeruginosa* biofilm response to UV-C irradiation: continuous UV-C irradiance that (a) *poorly inhibited* (UV-C < 3 μW/cm^2) and (b) *effectively inhibited* (8 μW/cm^2 < UV-C < 80 μW/cm^2) biofilm growth; (c) *P. aeruginosa* biofilm response to post-treatment by >250 μW/cm^2 UV-C light for 30 min.

encoding genes (−3.4 to 0-log$_2$fold) for biofilms in the *effectively inhibited* regions suggests that bacteria were not as likely to adhere to the surface. Hence, ample UV-C irradiation prevents bacterial attachment to the surface, supporting the earlier observation that OCT imaging revealed a reduced average biofilm thickness. In contrast, the pili- and fimbriae-encoding genes were upregulated by 0.1- to 1.2-log$_2$fold for biofilms in the *poorly inhibited* regions, which suggests that a lower UV-C intensity promoted adherence to the surface. These responses suggest that limiting the bacteria's mobility could be a potentially effective means of mitigating biofilm.

3.3.4. Integration of RNA Responses from Biofilms with Exposure to UV-C. The diagram in Figure 4 summarizes how *P. aeruginosa* biofilms responded to varying intensities of UV-C irradiation based on the mRNA results. To avoid stress from UV-C irradiation, the bacteria cells expended energy to move away from a higher UV-C exposure, but they formed a biofilm in lower UV-C exposure areas. While high-intensity UV-C severely inhibited biofilm growth, insufficient UV-C triggered an SOS response and quorum sensing of *P. aeruginosa* that eventually promoted biofilm formation. Thus, the dramatically different transcriptional responses of biofilm to UV-C indicate that the intensity needs to be precisely controlled when UV-C is used for biofilm inhibition. The observed trends in RNA responses suggested that future mechanistic studies of UV-C biofilm inhibition should focus on DNA repair, polysaccharide biosynthesis, and bacterial mobile organelles. A deeper understanding of the bacteria's defense mechanisms could lead to more efficient biofilm mitigation strategies.

4. ENVIRONMENTAL IMPLICATIONS

A major barrier in most biofilm applications with UV-C light is how to deliver light to surfaces where biofilms exist. For the first time, UV-C SEOFs were applied to a pressurized water system with flowing water. These conditions closely mimic real-world conditions of live planktonic bacteria being continuously deposited to surfaces where biofilms could colonize as well as resulting in hydraulic shear of live or inactivated cells and biofilm materials from the surface. Investigating the relationship between the biofilm growth rate and UV-C inhibiting rate in this system suggested that three crucial regimes can occur in systems relying upon UV-C light for biofilm control. Effective inhibition zones have sufficient UV-C light intensity (e.g., 8 μW/cm^2 with growth media and *P. aeruginosa* planktonic level) to avoid biofilm formation. A transitional zone, where biofilms may form and bacteria on the surface experience ROS stress and have physiological responses that may help mitigate UV-C damage, exists (e.g., approximately 3 to 8 μW/cm^2). Lower UV-C intensities appear to be ineffective in curtailing the growth of biofilms. The three ranges of UV-C intensities may not be universal to any water system and likely depend upon the types of bacteria, nutrient conditions, transmittance of the water, water temperature, fluid shear, and mode of light delivery (e.g., continuous versus intermittent duty cycling of light).[23] Additional research is needed on biofilm responses to UV-C light in general and specifically responses in flowing water systems.

There is increasing recognition that biofilms in pressurized water systems pose both operational challenges (e.g., membrane fouling, clogging of valves, fouling of sensor surfaces, unaesthetic particulates in drinking water) and potential health risks from opportunistic pathogens that reside within biofilms (e.g., *Nontuberculous Mycobacteria*, *Legionella pneumophila*, or *Pseudomonas aeruginosa*). The practical utilization of UV-C light for managing biofilms in dynamic water systems (such as municipal or facility plumbing networks, point-of-use devices, and hot-water storage tanks) is rapidly gaining traction in real-world scenarios. The main reason for limited research and products in this area is that traditional low-pressure lamps do not work well in narrow channels and shapes. But now, UV-C LEDs are quickly

https://doi.org/10.1021/acs.est.3c04658
Environ. Sci. Technol. 2023, 57, 15736−15746

becoming available at a low cost. UV-C LEDs are not only being used in systems that disinfect flowing water, but there are also patents and products that use LEDs in household faucets and shower fixtures. These LEDs are often arranged in waterproof polymers and irradiate only small surface areas. Attaching LEDs to SEOFs described herein offers a new design strategy to deliver light to large surface areas in narrow or curved channels. While the focus herein is on UV-C light inactivation, optical fibers with catalytic surfaces that produce reactive oxygen species (ROS) via photocatalysis have been proposed suitable for application in other geometries, including their use as spacers to prevent biofilms from fouling membrane surfaces.[42−44] Future research should continue to explore and improve strategies to utilize optical fibers with different surface coatings to mitigate biofilm-associated water quality problems.

An emerging and critical research need is the adoption of uniform terminology for different degrees of biofilm control (e.g., inhibition of growth, destruction of existing biofilms, sterilization) and associating these with operational challenges or health risks. Sterilization (i.e., no biofilms) is likely an unachievable goal in flowing water systems where planktonic sources of bacteria are always present. The closest one that may be able to achieve, approaching sterilization, would be providing continuous UV-C irradiation of all surfaces with high light intensities. Inhibiting biofilms with UV-C light is likely achievable when the rate of bacterial inactivation exceeds the rate of bacterial growth. How bacteria in biofilms respond differently to continuous versus intermittent UV-C irradiance is poorly understood, as is the contrast between high-intensity short duration (intermittent irradiation) and low-intensity continuous irradiation. Bacteria have various response and repair mechanisms that could influence biofilm formation in ways that differ significantly from the wealth of knowledge published on planktonic bacteria in the development of design criteria for drinking water disinfection. Estimates of UV-intensity required to inhibit biofilms may be achieved through controlled laboratory experiments using a collimated beam apparatus and mechanistic studies. Such studies could relate the prerequisites for log-inactivation and population thresholds of bacteria required for the initiation and sustenance of biofilms. However, as our findings demonstrate, once biofilms form on a surface, UV-C light may only partially hinder bacterial growth, providing only sufficient light to trigger the activation of genes responsible for EPS production or the construction of biofilm structures that obstruct light from reaching viable bacteria. Research is needed to understand the behavior of light within different components of live/dead bacteria but also within EPS, proteins, and other materials potentially present in biofilms. The dynamic nature of biofilms and their response to low levels of UV-C light are potentially one of the most critical areas for future research.

■ ASSOCIATED CONTENT

Supporting Information

The Supporting Information is available free of charge at https://pubs.acs.org/doi/10.1021/acs.est.3c04658.

Characteristics of feedwater medium (M9) used for biofilm-forming experiments (Table SI.1); details of RNA sequencing sample collection and sequencing quality control (Tables SI.2 and SI.3); experimental setup (Figure SI.1); schematic of light measurement by the spectroradiometer (Figure SI.2); pictures of UV-C LED glowing from the optical fiber inside the reactor (Figure SI.3); feedwater concentration during the recirculation (Figure SI.4); schematic of RNA sequencing sample collection (Figure SI.5); heatmap of light irradiance at 0-, 0.5, 1.0-, 1.5-, and 2.0 cm distance away from fiber surface (Figure SI.6); 3D OCT images of the biofilm on the surface inside the reactor (Figure SI.7); biofilm formation on the optical fiber surface (Figure SI.8); summary of biofilm average thickness (mm) in the 50 cm reactor where SEOFs delivered different UV-C irradiance levels across the reactor surface (Figure SI.9); CLSM images of the collected biofilm at areas where biofilm gets *effectively* or *poorly inhibited* (Figure SI.10) (PDF)

■ AUTHOR INFORMATION

Corresponding Authors

Paul Westerhoff − *NSF Nanosystems Engineering Research Center for Nanotechnology-Enabled Water Treatment, School of Sustainable Engineering and the Built Environment, Ira A. Fulton Schools of Engineering, Arizona State University, Tempe, Arizona 85287-3005, United States*; Email: p.westerhoff@asu.edu

Yi-Hao Luo − *NSF Nanosystems Engineering Research Center for Nanotechnology-Enabled Water Treatment, School of Sustainable Engineering and the Built Environment, Ira A. Fulton Schools of Engineering, Arizona State University, Tempe, Arizona 85287-3005, United States; Biodesign Swette Center for Environmental Biotechnology, Arizona State University, Tempe, Arizona 85287-5701, United States; Engineering Research Center of Low-Carbon Treatment and Green Development of Polluted Water in Northeast China, Northeast Normal University, Changchun 130117, China*; Email: yluo93@asu.edu

Authors

Zhe Zhao − *NSF Nanosystems Engineering Research Center for Nanotechnology-Enabled Water Treatment, School of Sustainable Engineering and the Built Environment, Ira A. Fulton Schools of Engineering, Arizona State University, Tempe, Arizona 85287-3005, United States*

Tzu-Heng Wang − *NSF Nanosystems Engineering Research Center for Nanotechnology-Enabled Water Treatment, School of Sustainable Engineering and the Built Environment, Ira A. Fulton Schools of Engineering, Arizona State University, Tempe, Arizona 85287-3005, United States*

Shahnawaz Sinha − *NSF Nanosystems Engineering Research Center for Nanotechnology-Enabled Water Treatment, School of Sustainable Engineering and the Built Environment, Ira A. Fulton Schools of Engineering, Arizona State University, Tempe, Arizona 85287-3005, United States*

Li Ling − *Advanced Interdisciplinary Institute of Environment and Ecology, Beijing Normal University, Zhuhai 519087, China*; orcid.org/0000-0003-2335-6969

Bruce Rittmann − *NSF Nanosystems Engineering Research Center for Nanotechnology-Enabled Water Treatment, School of Sustainable Engineering and the Built Environment, Ira A. Fulton Schools of Engineering, Arizona State University, Tempe, Arizona 85287-3005, United States; Biodesign Swette Center for Environmental Biotechnology, Arizona State University, Tempe, Arizona 85287-5701, United States*; orcid.org/0000-0002-3678-149X

https://doi.org/10.1021/acs.est.3c04658
Environ. Sci. Technol. 2023, 57, 15736−15746

Pedro Alvarez − *Department of Civil and Environmental Engineering, Rice University, Houston, Texas 77005, United States;* orcid.org/0000-0002-6725-7199

François Perreault − *NSF Nanosystems Engineering Research Center for Nanotechnology-Enabled Water Treatment, School of Sustainable Engineering and the Built Environment, Ira A. Fulton Schools of Engineering, Arizona State University, Tempe, Arizona 85287-3005, United States;* orcid.org/0000-0002-4756-8205

Complete contact information is available at: https://pubs.acs.org/10.1021/acs.est.3c04658

Notes

The authors declare no competing financial interest.

■ ACKNOWLEDGMENTS

This work was partially funded by the National Science Foundation Nanosystems Engineering Research Center for Nanotechnology-Enabled Water Treatment (EEC-1449500) and NASA (80NSSC19C0564). We would like to acknowledge the Eyring Materials Center at Arizona State University supported in part by the National Science Foundation (ECCS-1542160). Laurel Passantino provided technical editing.

■ REFERENCES

(1) Flemming, H.-C.; Wingender, J. The biofilm matrix. *Nature Reviews Microbiology* **2010**, *8* (9), 623−633.

(2) Cámara, M.; Green, W.; MacPhee, C. E.; Rakowska, P. D.; Raval, R.; Richardson, M. C.; Slater-Jefferies, J.; Steventon, K.; Webb, J. S. Economic significance of biofilms: a multidisciplinary and cross-sectoral challenge. *npj Biofilms and Microbiomes* **2022**, *8* (1), 42.

(3) Beck, S. E.; Rodriguez, R. A.; Linden, K. G.; Hargy, T. M.; Larason, T. C.; Wright, H. B. Wavelength Dependent UV Inactivation and DNA Damage of Adenovirus as Measured by Cell Culture Infectivity and Long Range Quantitative PCR. *Environ. Sci. Technol.* **2014**, *48* (1), 591−598.

(4) Ma, B.; Seyedi, S.; Wells, E.; McCarthy, D.; Crosbie, N.; Linden, K. G. Inactivation of biofilm-bound bacterial cells using irradiation across UVC wavelengths. *Water research (Oxford)* **2022**, *217*, 118379−118379.

(5) Luo, X.; Zhang, B.; Lu, Y.; Mei, Y.; Shen, L. Advances in application of ultraviolet irradiation for biofilm control in water and wastewater infrastructure. *Journal of Hazardous Materials* **2022**, *421*, 126682.

(6) Yuan, Q.; Yu, P.; Cheng, Y.; Zuo, P.; Xu, Y.; Cui, Y.; Luo, Y.; Alvarez, P. J. J. Chlorination (but Not UV Disinfection) Generates Cell Debris that Increases Extracellular Antibiotic Resistance Gene Transfer via Proximal Adsorption to Recipients and Upregulated Transformation Genes. *Environ. Sci. Technol.* **2022**, *56* (23), 17166−17176.

(7) Torkzadeh, H.; Cates, E. L. Biofilm growth under continuous UVC irradiation: Quantitative effects of growth conditions and growth time on intensity response parameters. *Water research (Oxford)* **2021**, *206*, 117747−117747.

(8) Torkzadeh, H.; Zodrow, K. R.; Bridges, W. C.; Cates, E. L. Quantification and modeling of the response of surface biofilm growth to continuous low intensity UVC irradiation. *Water research (Oxford)* **2021**, *193*, 116895−116895.

(9) Prado, D. B. d.; Szczerepa, M. M. d. A.; Capeloto, O. A.; Astrath, N. G. C.; Santos, N. C. A. d.; Previdelli, I. T. S.; Nakamura, C. V.; Mikcha, J. M. G.; Abreu Filho, B. A. d. Effect of ultraviolet (UV-C) radiation on spores and biofilms of Alicyclobacillus spp. in industrialized orange juice. *International journal of food microbiology* **2019**, *305*, 108238−108238.

(10) Bak, J.; Ladefoged, S. D.; Tvede, M.; Begovic, T.; Gregersen, A. Dose requirements for UVC disinfection of catheter biofilms. *Biofouling* **2009**, *25* (4), 289−296.

(11) Liu, S.; Wang, C.; Hou, J.; Wang, P.; Miao, L.; Fan, X.; You, G.; Xu, Y. Effects of Ag and Ag2S nanoparticles on denitrification in sediments. *Water research (Oxford)* **2018**, *137*, 28−36.

(12) Agathokleous, E.; Barceló, D.; Iavicoli, I.; Tsatsakis, A.; Calabrese, E. J. Disinfectant-induced hormesis: An unknown environmental threat of the application of disinfectants to prevent SARS-CoV-2 infection during the COVID-19 pandemic? *Environ. Pollut.* **2022**, *292*, 118429.

(13) Zhao, Z.; Lanzarini-Lopes, M.; Westerhoff, E.; Long, X.; Rho, H.; Bi, Y.; Ling, L.; Westerhoff, P. Evanescent wave interactions with nanoparticles on optical fiber modulate side emission of germicidal ultraviolet light. *Environmental science. Nano* **2021**, *8* (9), 2441−2452.

(14) Lanzarini-Lopes, M.; Zhao, Z.; Perreault, F.; Garcia-Segura, S.; Westerhoff, P. Germicidal glowsticks: Side-emitting optical fibers inhibit Pseudomonas aeruginosa and Escherichia coli on surfaces. *Water research (Oxford)* **2020**, *184*, 116191−116191.

(15) Lanzarini-Lopes, M.; Cruz, B.; Garcia-Segura, S.; Alum, A.; Abbaszadegan, M.; Westerhoff, P. Nanoparticle and Transparent Polymer Coatings Enable UV-C Side-Emission Optical Fibers for Inactivation of Escherichia coli in Water. *Environ. Sci. Technol.* **2019**, *53* (18), 10880−10887.

(16) Rho, H.; Yu, P.; Zhao, Z.; Lee, C.-S.; Chon, K.; Perreault, F.; Alvarez, P. J.; Amy, G.; Westerhoff, P. Inhibition of biofouling on reverse osmosis membrane surfaces by germicidal ultraviolet light side-emitting optical fibers. *Water Res.* **2022**, *224*, 119094.

(17) Song, Y.; Ling, L.; Westerhoff, P.; Shang, C. Evanescent waves modulate energy efficiency of photocatalysis within TiO2 coated optical fibers illuminated using LEDs. *Nat. Commun.* **2021**, *12* (1), 4101.

(18) Westerhoff, P.; Alvarez, P. J. J.; Kim, J.; Li, Q.; Alabastri, A.; Halas, N. J.; Villagran, D.; Zimmerman, J.; Wong, M. S. Utilizing the broad electromagnetic spectrum and unique nanoscale properties for chemical-free water treatment. *Current opinion in chemical engineering* **2021**, *33*, 100709.

(19) Wang, H.; Edwards, M. A.; Falkinham, J. O., III; Pruden, A. Probiotic Approach to Pathogen Control in Premise Plumbing Systems? A Review. *Environ. Sci. Technol.* **2013**, *47* (18), 10117−10128.

(20) Gheorghita, A. A.; Li, Y. E.; Kitova, E. N.; Bui, D. T.; Pfoh, R.; Low, K. E.; Whitfield, G. B.; Walvoort, M. T. C.; Zhang, Q.; Codée, J. D. C.; Klassen, J. S.; Howell, P. L. Structure of the AlgKX modification and secretion complex required for alginate production and biofilm attachment in Pseudomonas aeruginosa. *Nat. Commun.* **2022**, *13* (1), 7631.

(21) Demir, B.; Taylor, A.; Broughton, R. M.; Huang, T. S.; Bozack, M. J.; Worley, S. D. N-halamine surface coating for mitigation of biofilm and microbial contamination in water systems for space travel. *Biofilm* **2022**, *4*, 100076−100076.

(22) Mettler, M. K.; Parker, C. W.; Venkateswaran, K.; Peyton, B. M. Antimicrobial Coating Efficacy for Prevention of Pseudomonas aeruginosa Biofilm Growth on ISS Water System Materials. *Frontiers in microbiology* **2022**, *13*, 874236−874236.

(23) Zhao, Z.; Rho, H.; Shapiro, N.; Ling, L.; Perreault, F.; Rittmann, B.; Westerhoff, P. Biofilm inhibition on surfaces by ultraviolet light side-emitted from optical fibres. *Nature Water* **2023**, *1* (7), 649−657.

(24) Bolger, A. M.; Lohse, M.; Usadel, B. Trimmomatic: A flexible trimmer for Illumina sequence data. *BIOINFORMATICS* **2014**, *30* (15), 2114−2120.

(25) Meinicke, P. UProC: Tools for ultra-fast protein domain classification. *BIOINFORMATICS* **2015**, *31* (9), 1382−1388.

(26) Wagner, G. P.; Kin, K.; Lynch, V. J. Measurement of mRNA abundance using RNA-seq data: RPKM measure is inconsistent among samples. *Theory Biosci.* **2012**, *131* (4), 281−285.

(27) Inurria, A.; Cay-Durgun, P.; Rice, D.; Zhang, H.; Seo, D.-K.; Lind, M. L.; Perreault, F. Polyamide thin-film nanocomposite

membranes with graphene oxide nanosheets: Balancing membrane performance and fouling propensity. *Desalination* **2019**, *451*, 139−147.
(28) Rho, H.; Im, S.-J.; Alrehaili, O.; Lee, S.; Jang, A.; Perreault, F. o.; Westerhoff, P. Facile Surface Modification of Polyamide Membranes Using UV-Photooxidation Improves Permeability and Reduces Natural Organic Matter Fouling. *Environ. Sci. Technol.* **2021**, *55* (10), 6984−6994.
(29) Dötsch, A.; Eckweiler, D.; Schniederjans, M.; Zimmermann, A.; Jensen, V.; Scharfe, M.; Geffers, R.; Häussler, S. The pseudomonas aeruginosa transcriptome in planktonic cultures and static biofilms using rna sequencing. *PloS One* **2012**, *7* (2), No. e31092.
(30) Erill, I.; Campoy, S.; Barbé, J. Aeons of distress: an evolutionary perspective on the bacterial SOS response. *FEMS microbiology reviews* **2007**, *31* (6), 637−656.
(31) Walker, G. C. SOS response of *Escherichia coli*. In *Escherichia coli and Salmonella: Cellular and Molecular Biology*; ASM Press, 1996.
(32) Zhang, X.; Lee, K.; Yu, H.; Mameda, N.; Choo, K.-H. Photolytic quorum quenching: A new anti-biofouling strategy for membrane bioreactors. *Chemical engineering journal (Lausanne, Switzerland: 1996)* **2019**, *378*, 122235.
(33) Schuster, M.; Peter Greenberg, E. A network of networks: Quorum-sensing gene regulation in Pseudomonas aeruginosa. *International journal of medical microbiology* **2006**, *296* (2), 73−81.
(34) Diggle, S. P.; Stacey, R. E.; Dodd, C.; Cámara, M.; Williams, P.; Winzer, K. The galactophilic lectin, LecA, contributes to biofilm development in Pseudomonas aeruginosa. *Environmental microbiology* **2006**, *8* (6), 1095−1104.
(35) Tielker, D.; Hacker, S.; Loris, R.; Strathmann, M.; Wingender, J.; Wilhelm, S.; Rosenau, F.; Jaeger, K.-E. Pseudomonas aeruginosa lectin LecB is located in the outer membrane and is involved in biofilm formation. *Microbiology (Society for General Microbiology)* **2005**, *151* (5), 1313−1323.
(36) Murphy, K.; Park, A. J.; Hao, Y.; Brewer, D.; Lam, J. S.; Khursigara, C. M. Influence of O Polysaccharides on Biofilm Development and Outer Membrane Vesicle Biogenesis in Pseudomonas aeruginosa PAO1. *Journal of bacteriology* **2014**, *196* (7), 1306−1317.
(37) Williams, V.; Fletcher, M. Pseudomonas fluorescens adhesion and transport through porous media are affected by lipopolysaccharide composition. *Appl. Environ. Microbiol.* **1996**, *62* (1), 100−104.
(38) Chen, S.; Beeby, M.; Murphy, G. E.; Leadbetter, J. R.; Hendrixson, D. R.; Briegel, A.; Li, Z.; Shi, J.; Tocheva, E. I.; Müller, A.; Dobro, M. J.; Jensen, G. J. Structural diversity of bacterial flagellar motors. *EMBO journal* **2011**, *30* (14), 2972−2981.
(39) Smith, W. P. J.; Wucher, B. R.; Nadell, C. D.; Foster, K. R. Bacterial defences: mechanisms, evolution and antimicrobial resistance. *Nature Reviews Microbiology* **2023**, *21* (8), 519−534.
(40) Craig, L.; Forest, K. T.; Maier, B. Type IV pili: dynamics, biophysics and functional consequences. *Nature reviews. Microbiology* **2019**, *17* (7), 429−440.
(41) Tuomola, E. M.; Ouwehand, A. C.; Salminen, S. J. The effect of probiotic bacteria on the adhesion of pathogens to human intestinal mucus. *FEMS immunology and medical microbiology* **1999**, *26* (2), 137−142.
(42) Ni, L.; Wang, K.; Wang, Z.; Wang, Y. Antibiofouling Characteristics and Mechanisms in an Anammox Membrane Bioreactor Based on an Optimized Photocatalytic Technology−Photocatalytic Optical Fibers. *Environ. Sci. Technol.* **2022**, *56* (22), 16144−16155.
(43) Ni, L.; Wang, T.; Wang, K.; Ma, J.; Wang, Y. Novel Control Strategy for Membrane Biofouling by Surface Loading of Aerobically and Anaerobically Applicable Photocatalytic Optical Fibers Based on a Z-Scheme Heterostructure Zr-MOFs/rGO/Ag3PO4 Photocatalyst. *Environ. Sci. Technol.* **2022**, *56* (10), 6608−6620.
(44) Cheng, Z.; Shang, C.; Westerhoff, P.; Ling, L. Novel polymer optical fibers with high mass-loading g-C3N4 embedded metamaterial porous structures achieve rapid micropollutant degradation in water. *Water Res.* **2023**, *242*, 120234.

https://doi.org/10.1021/acs.est.3c04658
Environ. Sci. Technol. 2023, 57, 15736−15746